View metadata, citation and similar papers at core.ac.uk
brought to you by CORE
provided by Apollo

1 # Effect of bore fluid composition on microstructure and performance of a
2 # microporous hollow fibre membrane as a cation-exchange substrate

3

4 R. A. Lazar, I. Mandal, N.K.H. Slater*

5

6 Department of Chemical Engineering and Biotechnology, University of Cambridge, Pembroke Street,
7 Cambridge, CB2 3RA, United Kingdom

8

9 *Corresponding author. Tel.: +44 (0) 1223 762953; Fax: +44 (0) 1223 334796
10 Email address: nkhs2@cam.ac.uk (N. Slater)

11
12
13
14
15
16
17
18
19
20
21
22
23
24
25
26
27
28
29
30
31
32
33
34
35
36
37

Abstract

Micro-capillary film (MCF) membranes are effective platforms for bioseparations and viable alternatives to established packed bed and membrane substrates at the analytical and preparative chromatography scales. Single hollow fibre (HF) MCF membranes with varied microstructures were produced in order to evaluate the effect of the bore fluid composition used during hollow fibre extrusion on their structure and performance as cation-exchange adsorbers. Hollow fibres were fabricated from ethylene-vinyl alcohol (EVOH) copolymer through solution extrusion followed by nonsolvent induced phase separation (NIPS) using bore fluids of differing composition (100 wt.% N-methyl-2-pyrrolidone (NMP), 100 wt.% glycerol, 100 wt.% water). All HFs displayed highly microporous and mesoporous microstructures, with distinct regions of pore size <1 μm, 5-15 μm and up to 50 μm in diameter, depending upon proximity to the bore fluid. Scanning electron microscopy (SEM) revealed skins of pore size <1 μm at the inner surface of HFs produced with water and glycerol, while NMP bore fluid resulted in a skinless inner HF surface. The HFs were modified for chromatography by functionalising the polymer surface hydroxyl groups with sulphonic acid (SP) groups to produce cation-exchange adsorbers. The maximum binding capacities of the HFs were determined by frontal analysis using lysozyme solutions (0.05 mg ml^{-1} to 100 mg ml^{-1}) for a flow rate of 1.0 ml min^{-1}. The NMP-HF-SP module displayed the largest maximum lysozyme binding capacity of all the fibres produced (40.3 mg lysozyme/ml adsorbent volume), a nearly 2-fold increase over the glycerol and 13-fold increase over the water variants at the same sample flow rate. The importance of NMP as a bore fluid to hollow fibre membrane performance as a result of inner surface porosity was established with a view to applying this parameter for the optimisation of multi-capillary MCF performance in future studies.

Keywords

Cation-exchange, Ion-exchange, Chromatography, Hollow fibre, Microporous, Separation

75 **1. Introduction**
76
77 Ion-exchange chromatography is widely used in the downstream processing of
78 biopharmaceuticals as it provides high-resolution separation of biomolecules from mixtures
79 based on net charge. The two most commonly used approaches in ion-exchange
80 chromatography, packed bed columns and membrane adsorbers, have high binding
81 capacities and good separation characteristics [1]. However, packed bed columns usually
82 operate under low column flow rates due to bed compression, high pressure drops and low
83 mass transfer rates as diffusion is the primary mode of analyte transport to binding sites
84 within the bed pores [2]. In order to overcome this limitation, membrane adsorbers have
85 been developed in which analyte transport to binding sites depends primarily on convection,
86 thus allowing separations to run at higher flow rates without compromising performance.
87 Typically, membranes have lower pressure drops and offer independence of binding
88 capacity from flow rate [3], although generally exhibit lower binding capacities than packed
89 beds [2].
90
91 Micro-capillary film (MCF) membranes have been demonstrated to be effective platforms for
92 bioseparations and viable alternatives to established chromatography substrates at the
93 analytical and preparative scales, as they offer good binding capacities with high superficial
94 flow rates, low pressure drops and do not involve column packing operations [1,4,5]. MCFs
95 are microstructured membranes containing continuous capillaries embedded within a flat
96 polymer film, with the number of capillaries depending on the die used during the
97 manufacturing process. Both nonporous MCFs (NMCFs) and microporous MCFs (MMCFs)
98 have been produced from ethylene-vinyl alcohol copolymer (EVOH) through extrusion
99 processes [6,7]. Taking advantage of the hydrophilic nature of EVOH and its exposed
100 hydroxyl group, the MCF membrane surfaces can be functionalised into adsorbent surfaces
101 via conjugation of functional ligands to the polymer [4]. Previously, the nonporous NMCF
102 was used as a cation-exchange membrane adsorber for lysozyme purification [4] and as an
103 anion-exchange membrane adsorber for lentivirus capture from cell culture [1]. The use of
104 porous MMCF as a cation-exchange adsorber for bioseparations has also been
105 demonstrated [5].
106
107 MMCFs offer distinct advantages over NMCFs. Due to their porous structure, the MMCF
108 surface area available for functionalisation is greatly increased, resulting in a 10^4 fold higher
109 binding capacity compared to NMCF in membranes functionalised for cation-exchange
110 chromatography [5]. In addition, bioseparations can be run at high superficial flow velocities
111 while withstanding low pressure drops. It has been demonstrated that the binding capacity of

112 MMCF is comparable to commercially available packed bed and membrane adsorbers, while
113 providing a sharp breakthrough and higher throughput and pressure tolerance than that of
114 currently available preparative scale purification substrates [5]. The potential of MMCF in
115 terms of binding capacity can be further enhanced by altering key parameters in the
116 membrane manufacturing process. Parameters such as dope composition, bore fluid
117 composition, polymer and bore fluid flow rate, air gap distance to coagulant, take-up rate,
118 and extrusion temperature have been shown to affect membrane characteristics [8,9,10]. In
119 particular, the composition of the bore fluid has been shown to affect membrane morphology
120 [11] and adsorption performance [12].
121
122 Previously, MMCF has been proven to be a suitable chromatography substrate [5]. However,
123 MMCF manufacturing conditions have yet to be optimised for improved chromatographic
124 performance. The main objective here is to evaluate the effect of bore fluid composition
125 during MMCF fabrication on the morphology and performance of an EVOH hollow fibre
126 MMCF as a cation-exchange adsorber. The single hollow fibre (HF) membrane variant of
127 MMCF was chosen as a test system due to its symmetry and relative geometrical simplicity
128 compared to the multi-capillary MMCF extruded with a 19-nozzle die used in the studies
129 described previously [5]. Since HFs were produced through a nonsolvent induced phase
130 separation process (NIPS), the varying solubility of the bore fluid used to form the central
131 capillary of the hollow fibre affected the speed of polymer phase separation into this
132 coagulant. This in turn altered the morphology and porous microstructure that was observed
133 with SEM, as it changed the rate of polymer precipitation at the coagulant interface. The
134 extruded HFs were then functionalised into cation-exchange chromatography modules and
135 their performance as cation-exchange adsorbers was evaluated.
136

137 2. Materials and methods

138

139 *2.1 Chemicals and reagents*

140
141 Ethylene-vinyl alcohol copolymer (EVOH) containing 32 mol% ethylene was supplied by
142 Kuraray (Hattersheim, Germany). N-methyl-2-pyrrolidone (NMP), polyvinylpyrrolidone (PVP,
143 avg. mol wt. 360,000), glycerol, anhydrous NaOH, cyanuric chloride, acetone, Na_2HPO_4, 3-
144 amino-1-propanesulphonic acid, crystalline tris(hydroxymethyl)aminomethane (Tris), HCl
145 and crystalline chick-egg lysozyme were supplied by Sigma Aldrich (St. Louis, MO, USA). All
146 chemicals and biochemicals used were of analytical grade.
147

148 *2.2 Extrusion and assembly of hollow fibre module*

149
150 Hollow fibre (HF) membranes were extruded from EVOH via nonsolvent induced phase
151 separation (NIPS) according to a protocol described by Bonyadi and Mackley [7]. Briefly,
152 polymer solutions containing 15/10/75 wt.% EVOH/PVP/NMP were extruded (polymer
153 solution flow rate of 1.5 ml min^{-1}) at ambient temperature through an annular die into a water
154 coagulation bath along with one of three different entrained bore fluids (bore fluid flow rate
155 0.5 ml min^{-1}). An air gap of 0.5 cm and take-up speed of 75.4 cm min^{-1} were used. 100 wt.%
156 bore fluids of water, glycerol and NMP were used to manipulate fibre microstructure by
157 altering polymer precipitation rates across the membranes (**Fig.1**). NMP and water are
158 similar in viscosity and density [11], while glycerol is denser and more viscous. At the
159 concentrations used in this study, EVOH was completely soluble in NMP, sparingly soluble
160 in glycerol and insoluble in water, based on each compound's Hansen solubility parameters.
161 The HFs were adapted into chromatography columns by encasing 10 cm long sections of HF
162 within 6.35 mm diameter FEP plastic tubing (Kinesis Ltd., St. Neots, UK) using epoxy glue
163 purchased from Huntsman (Araldite®, Cleveland, OH, USA). Upchurch 1/4 in. HPLC
164 connectors were placed at the column ends and were attached to an ÄKTA FPLC system
165 (GE Healthcare Life Sciences, Uppsala, SWE). The ÄKTA FPLC was used to pump various
166 buffers and protein solutions axially through the HF module lumen. There was no radial flow
167 through the fibres as they were encased in epoxy.
168
169 *2.3 Scanning electron microscopy (SEM) and mercury intrusion porosimetry*
170
171 SEM samples were fractured in liquid nitrogen, freeze-dried starting at -90 ºC in a Quorum
172 K775X freeze dryer (Laughton, UK) and sputter coated in platinum in order to obtain sharp
173 membrane cross-sections for imaging. Surface and cross-sections of HF samples were
174 imaged using an FEI Verios 460 scanning electron microscope (FEI, USA) operated at 5 kV.
175 Membrane pore surface area was measured by mercury intrusion porosimetry using a
176 Micromeritics AutoPore IV 9500 porosimeter (Norcross, GA, USA).
177
178 *2.4 Surface modification of HF modules with SP groups*
179
180 The surface of the HF modules was adapted into a cation-exchange chromatography
181 adsorber using protocols established by Darton [4] and McCreath [13]. Briefly, the
182 nucleophilicity of the HF membrane surface was increased by flowing 30 ml of 1 M NaOH for
183 30 min through the module using a Knauer Smartline 100 HPLC pump (Berlin, DE). Next, a
184 linker group was added by flowing 20 ml of 50 mM cyanuric chloride in acetone solution for
185 20 min. After a 10 min wash with 10 ml of MilliQ water, sulphonic acid (SP) groups were

186 covalently attached to the linker by recirculating 20 ml of a 1 M solution of Na_2HPO_4
187 containing 1 g of 3-amino-1-propanesulphonic acid overnight in a 60˚C water bath. Finally,
188 the column was washed with 20 ml MilliQ water for 20 min, 20 ml NaOH in water (0.4 M) for
189 20 min, and again 20 ml MilliQ water for 20 min. Hereafter, the SP functionalised HFs
190 produced with the three bore fluids water, glycerol and NMP will be referred to as water-HF-
191 SP, glycerol-HF-SP and NMP-HF-SP.
192
193 *2.5 Frontal analysis study and equilibrium binding capacity analysis*
194
195 Binding capacity analysis was carried out based on a methodology developed by Darton et
196 al. [4]. The HF modules were first pre-equilibrated with running buffer, 20 mM Tris-HCl pH
197 7.2, for at least 2 column volumes (column volume, CV, is defined as the total volume within
198 the microporous walls and the central capillary, 1 CV = 0.14 ml). The modules were then
199 continuously loaded with lysozyme (C_{inj} = 5.0 mg ml^{-1}) in 20 mM Tris-HCl pH 7.2 using a
200 Knauer Smartline 100 HPLC pump until the column was saturated based on UV absorbance
201 as measured by the ÄKTA FPLC system. When nearly 100% lysozyme breakthrough was
202 reached, the saturation UV absorbance height in optical density units at 280 nm was noted.
203 The module was then washed with running buffer and then eluted using a step gradient of 1
204 M NaCl in 20 mM Tris-HCl pH 7.2 solution to strip any bound protein. The module was then
205 re-equilibrated with running buffer. The absorbance during loading and elution at 280 nm
206 was monitored and integrated to calculate the amount of lysozyme bound and eluted. Tests
207 were conducted in triplicate at a sample flow rate of 1 ml min^{-1}. Pressure drops and binding
208 capacities across the modules were measured at flow rates of 1 , 2, 3, 4 and 5 ml min^{-1},
209 corresponding to superficial flow velocities through the fibre lumens ranging from 6,000 cm
210 h^{-1} to 175,000 cm h^{-1} (0.017 m s^{-1} to 0.486 m s^{-1}). The mass of protein eluted was then
211 calculated by:

$$Mass\ eluted\ (mg) = \frac{C_{inj}\ \left(\frac{mg}{ml}\right) \times Elution\ Area\ (mA.U.ml)}{100\ \%\ saturation\ height\ (mA.U.)} \tag{1}$$

212 To study the equilibrium binding capacity of the HFs, the above protocol was repeated at a
213 flow rate of 1 ml min^{-1} using lysozyme solutions with concentrations between 0.05 and 100
214 mg ml^{-1}. The equilibrium binding capacity was calculated using the Langmuir isotherm model
215 for adsorption on a ligand surface [14], which states:

$$\theta = \frac{\alpha C_{inj}}{1 + \alpha C_{inj}} \tag{2}$$

216 where θ is the fractional coverage of the surface, α is the Langmuir adsorption constant and
217 C_{inj} is the lysozyme concentration used at injection. The amount of protein being loaded, q, is
218 related to the maximum equilibrium amount bound, q_{max}, by [4]

$$q = \theta q_{max} \quad (3)$$

219 Combining Eqs. (2) and (3):

$$q = q_{max} \frac{\alpha C_{inj}}{1 + \alpha C_{inj}} \quad (2)$$

220 allows q_{max} to be calculated. This represents the maximum equilibrium binding capacity of
221 the HF membranes.
222

223 **3. Results and Discussion**

224

225 HF membrane cross-sections and internal surfaces were observed by SEM to identify
226 differences in microstructure caused by the bore fluid used. All membranes displayed a
227 sponge-like, macrovoid-free structure characteristic of phase separation by spinodal
228 decomposition [15], as seen in **Fig. 2**. The membranes showed ring-like bands of distinct
229 pore sizes within their cross-sections, suggesting regio-specific precipitation rates based on
230 proximity to the coagulant, either in the coagulation bath or bore fluid, and the type of
231 coagulant used. Dense skins of small pores (<1 μm diameter) were found in regions where
232 phase separation occurred fastest, such as in **Fig. 2(A)** at the inner and outer membrane
233 surfaces where the polymer dope came into contact with nonsolvent (water) as soon as it
234 was exposed to both the bore fluid and the coagulant bath. The largest pores, up to 50 μm
235 diameter, were found in regions where phase separation occurred slowest [16], as in **Fig.**
236 **2(C)** at the inner surface where the polymer contacted solvent NMP. At this surface, large
237 pores formed due to the presence of NMP in the bore fluid reducing the flux of solvent out of
238 the polymer solution [12]. Regions of intermediate pore size (5-15 μm) were found within the
239 membrane cross-sections where phase separation occurred at intermediate rates. At the
240 inner membrane surface, skins of pores <1 μm formed when glycerol and water were used
241 (**Fig. 2(A) & (B)**), whereas no skin was formed when NMP solvent was used, with pores
242 reaching 50 μm in diameter (**Fig. 2(C)**). The membrane pore surfaces areas available for
243 functionalisation with SP groups were similar for all three HFs (water, 6.07 m^2 g^{-1}; glycerol,
244 6.62 m^2 g^{-1}; NMP, 6.84 m^2 g^{-1}).
245

246 The NMP-HFs and glycerol-HFs displayed fully formed central circular capillaries. The highly
247 irregular inner membrane surface for water-HF seen in **Fig. 2(A)** may be attributable to a
248 buckling of the innermost region due to firstly, a rapid precipitation of this region caused by

249 exposure to water bore fluid prior to the HF entering the coagulation bath, and then further
250 volume shrinkage of the polymer-rich phase caused by precipitation of the remaining
251 membrane once the HF passed into the coagulation bath [11,17].
252
253 To test the effect of HF microstructure on membrane binding capacity performance as
254 cation-exchange adsorbers, lysozyme frontal analysis and Langmuir isotherm binding
255 capacity studies were conducted on the three HF-SP variants. Blank runs with HF modules
256 without surface modifications showed no protein adsorption. No membrane blocking or
257 fouling was observed. The pressure drop across the modules increased linearly with flow
258 rate (**Fig. 3(A)**). All pressure drops were below 0.35 MPa in the flow rate range (1-5 ml min^{-1})
259 typically used for commercial chromatography membranes (Pall Mustang® Q and S
260 membranes). However, in terms of HF membrane operation, these correspond to much
261 higher lumen superficial flow velocities (6,000 cm h^{-1} to 175,000 cm h^{-1}). Low pressure drops
262 at high superficial flow velocities indicate that HF MMCFs can be used for high throughput
263 studies. As expected, equilibrium lysozyme binding capacities were independent of the flow
264 rates tested (**Fig. 3(B)**).
265
266 A characteristic normalised breakthrough curve for lysozyme frontal analysis can be seen in
267 **Fig. 4**. The NMP-HF-SP module was able to bind and elute the largest amount of lysozyme,
268 while the water-HF-SP module bound and eluted the least. The NMP-HF-SP module
269 displayed the best performance as it bound the greatest mass of lysozyme (19.6 ± 2.64 mg
270 ml^{-1} adsorbent) at equilibrium among the modules tested when loaded with a 5 mg ml^{-1}
271 lysozyme solution, as shown by its large elute peak in **Fig. 4(B)**. When loaded to near
272 saturation and on subsequent elution, 88% of the protein bound was recovered in the eluent.
273 The water-HF-SP module bound the lowest amount of lysozyme (1.99 ± 0.17 mg ml^{-1}
274 adsorbent), while the glycerol-HF-SP module bound an intermediate amount of protein (9.73
275 ± 0.87 mg ml^{-1} adsorbent).
276
277 **Fig. 5** shows the mass of lysozyme bound to the HF modules based on different protein
278 loading concentrations. The NMP-HF-SP module displayed the largest lysozyme maximum
279 binding capacity (q_{max} = 40.3 mg ml^{-1} adsorbent), while the glycerol and water modules
280 bound less, 21.2 mg ml^{-1} adsorbent and 3.9 mg ml^{-1} adsorbent respectively. The Langmuir
281 isotherms fit the data well (R^2 values > 0.90), indicating that the lysozyme binds to all HF
282 membranes as a monolayer. All three HF modules had a lower lysozyme maximum binding
283 capacity than the 19-capillary MMCFs produced with glycerol bore fluid (64.7 mg ml^{-1}
284 adsorbent) [5] and might be attributed to the geometry of the MMCF module whose 19
285 parallel capillaries may provide better analyte access to the functionalised membrane

surface. In addition, the NIPS process during MMCF manufacture would be expected to produce different microstructures depending on the membrane geometry used. The size and shape of the membranes greatly affect phase separation kinetics within the membrane. Compared to commercial membrane substrates whose binding capacities typically exceed 50 mg ml^{-1} adsorbent (Pall Mustang® S), the HF membranes also have lower binding capacities. However, commercial membrane substrates are typically operated in a trans-membrane flow configuration, which may increase binding capacity.

In membrane adsorbers, the accessibility of the functionalised pore surface to analytes is key for good binding performance [18]. Since only axial convective flow is present in the HF module configuration tested, a more open pore structure at the inner membrane surface near the lumen is expected to provide better analyte access into the remaining porous mass. Smaller porosity near the lumen would reduce this access. The NMP-HF-SP module displayed the most open structure with the largest pores at the lumen surface. This module also had the highest equilibrium binding capacities at all tested loading concentrations, likely due to the NMP-HF-SP membrane presenting more accessible functional sites to lysozyme as a result of large porosity near the lumen. The small pores in the dense inner membrane surface of the water-HF-SP and glycerol-HF-SP modules are potentially the reason for the lower binding capacity evaluated. These dense skins offered a greater barrier to the analyte reaching and interacting with a large portion of the adsorptive surface.

4. Conclusions

In this study we have shown the importance of the bore fluid composition used during EVOH hollow fibre membrane manufacture to membrane microstructure and performance as a cation-exchange adsorber. Three bore fluids with varying solubility were used to produce HFs which were then functionalised into cation-exchange adsorbers. SEM micrographs revealed that NMP bore fluid produced a membrane with a skinless inner surface populated by large pores up to 50 µm in diameter. Glycerol and water bore fluids produced dense skins with much smaller pores at this inner membrane surface (<1 µm). Results of binding capacity studies indicated that NMP as an internal coagulant produced modules with the largest lysozyme maximum binding capacity, which corresponded with the fibres displaying the most open microstructure near the fibre lumen. This open microstructure caused by NMP bore fluid provided more accessible functional sites to lysozyme as an analyte. These findings can be further applied to optimise the inner surface microstructure in multi-capillary MMCFs by increasing bore fluid NMP concentration in order to obtain higher binding capacities and enhanced performance as chromatography substrates.

323

324 **Acknowledgments**

325 The authors would like to acknowledge the financial support of the University of Cambridge
326 CHESS scheme. The authors would like to thank Dr. Jeremy Skepper for help with SEM
327 imaging and assistance by Dr. Bart Hallmark and Matthew Townsend.

328

329 **References**

330 [1] N.J. Darton, D. Darling, M.J. Townsend, D.J. McNally, F. Farzaneh, N.K.H. Slater,
331 Lentivirus capture directly from cell culture with Q-functionalised microcapillary film
332 chromatography., Journal of Chromatography. A. 1251 (2012) 236–9.

333 [2] R. Ghosh, Protein separation using membrane chromatography: opportunities and
334 challenges., Journal of Chromatography. A. 952 (2002) 13–27.

335 [3] C. Charcosset, Review: purification of proteins by membrane chromatography,
336 Journal of Chemical Technology and Biotechnology. 71 (1998) 95–110.

337 [4] N.J. Darton, N.M. Reis, M.R. Mackley, N.K.H. Slater, Fast cation-exchange separation
338 of proteins in a plastic microcapillary disc., Journal of Chromatography. A. 1218
339 (2011) 1409–15.

340 [5] I. Mandal, M.J. Townsend, N.J. Darton, S. Bonyadi, N.K.H. Slater, A microporous
341 walled micro-capillary film module for cation-exchange protein chromatography,
342 Journal of Membrane Science. 466 (2014) 123–129.

343 [6] B. Hallmark, F. Gadala-Maria, M.R. Mackley, The melt processing of polymer
344 microcapillary film (MCF), Journal of Non-Newtonian Fluid Mechanics. 128 (2005) 83–
345 98.

346 [7] S. Bonyadi, M. Mackley, The development of novel micro-capillary film membranes,
347 Journal of Membrane Science. 389 (2012) 137–147.

348 [8] J. Qin, T. Chung, Effect of dope flow rate on the morphology, separation performance,
349 thermal and mechanical properties of ultrafiltration hollow fibre membranes, Journal of
350 Membrane Science. 157 (1999) 35–51.

351 [9] J. Ren, T. Chung, D. Li, R. Wang, Y. Liu, Development of asymmetric 6FDA-2,6 DAT
352 hollow fiber membranes for CO2/CH4 separation: 1. The influence of dope
353 composition and rheology on membrane morphology and separation performance,
354 Journal of Membrane Science. 207 (2002) 227–240.

355 [10] S. Deshmukh, K. Li, Effect of ethanol composition in water coagulation bath on
356 morphology of PVDF hollow fibre membranes, Journal of Membrane Science. 150
357 (1998) 75–85.

358 [11] S. Bonyadi, T.S. Chung, W.B. Krantz, Investigation of corrugation phenomenon in the
359 inner contour of hollow fibers during the non-solvent induced phase-separation
360 process, Journal of Membrane Science. 299 (2007) 200–210.

[12] M. Rahbari-sisakht, a. F. Ismail, T. Matsuura, Effect of bore fluid composition on structure and performance of asymmetric polysulfone hollow fiber membrane contactor for CO2 absorption, Separation and Purification Technology. 88 (2012) 99–106.

[13] G. McCreath, R. Owen, D. Nash, H. Chase, Preparation and use of ion-exchange chromatographic supports based on perfluoropolymers, Journal of Chromatography A. 773 (1997) 73–83.

[14] I. Langmuir, The Constitution and Fundamental Properties of Solids and Liquids, J. Am. Chem. Soc. 38 (1916) 2221–2295.

[15] R.W. Baker, Membrane Technology and Applications, John Wiley & Sons, Ltd, Chichester, UK, 2004.

[16] G.R. Guillen, Y. Pan, M. Li, E.M. V. Hoek, Preparation and Characterization of Membranes Formed by Nonsolvent Induced Phase Separation: A Review, Industrial & Engineering Chemistry Research. 50 (2011) 3798–3817.

[17] H. Tanaka, T. Araki, Viscoelastic phase separation in soft matter: Numerical-simulation study on its physical mechanism, Chemical Engineering Science. 61 (2006) 2108–2141.

[18] M. Ulbricht, Advanced functional polymer membranes, Polymer. 47 (2006) 2217–2262.

List of Figures

Fig. 1. Schematic diagram of the NIPS extrusion platform used to fabricate hollow fibre membranes.

Fig. 2. SEM images showing cross-sectional microstructure in hollow fibre membranes manufactured with three bore fluids: (A) water, (B) glycerol and (C) NMP

Fig. 3. Effect of flow rate on (A) pressure drop, *ΔP*, across the HF MMCF modules and (B) binding capacity of three HF-SP modules loaded to equilibrium. The mass of lysozyme bound per unit adsorbent volume is shown. Error bars represent the standard deviation of three replicates.

Fig. 4. Lysozyme breakthrough curves for HF membranes produced with three bore fluids (water, glycerol, NMP) and functionalised into cation-exchange chromatography modules via sulphonic acid surface modification (HF-SP). The modules were loaded to near saturation (A) with 5 mg ml^{-1} lysozyme in 20 mM Tris-HCl buffer (pH 7.2) for at least 15 column volumes (column volume, CV, is defined as the total volume within the microporous walls and the central capillary, 1 CV = 0.14 ml), washed with Tris-HCl running buffer to remove unbound protein and eluted (B) with 1 M NaCl in Tris-HCl running buffer for 80 column volumes to remove mass adsorbed to the membrane surface. All flow rates used were 1 ml min^{-1}. Protein absorbance at 280 nm and NaCl conductivity were measured. C/C_0 represents

403 the UV absorbance of the running lysozyme concentration, *C*, normalised by the feed
404 concentration, C_0.
405
406 **Fig. 5.** Ligand density model of HF modules. Lysozyme mass bound was measured at
407 different lysozyme loading concentrations, *C*, and binding data was fitted to a standard
408 Langmuir isotherm model. The dotted lines represent Langmuir isotherm equation fits and
409 give the following maximum equilibrium binding capacities (q_{max}): 40.3 mg ml^{-1} adsorbent
410 volume (NMP-HF-SP), 21.2 mg ml^{-1} adsorbent volume (glycerol-HF-SP) and 3.9 mg ml^{-1}
411 adsorbent volume (water-HF-SP). Error bars represent the standard deviation of three
412 replicates.

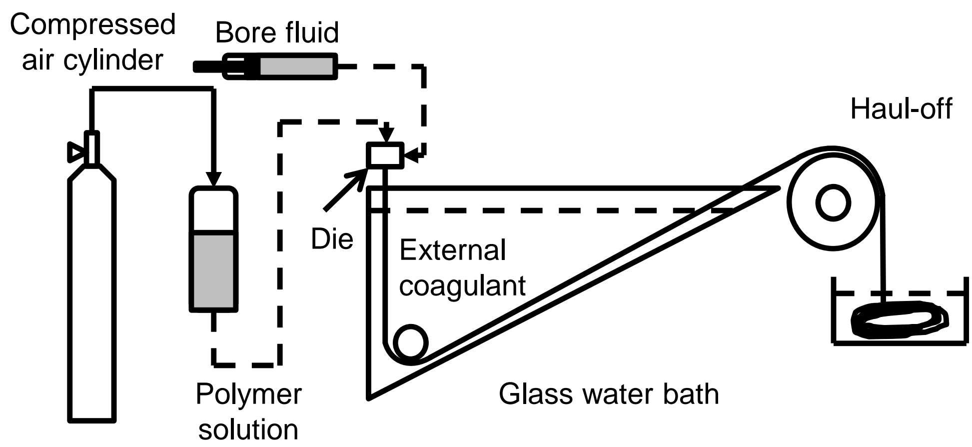
Compressed
air cylinder
Bore fluid
Haul-off
Die
External
coagulant
Polymer
solution
Glass water bath

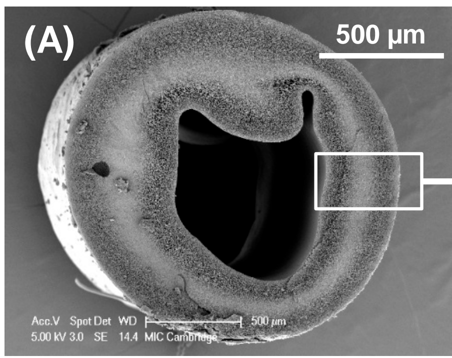
(A)
500 µm
Acc.V Spot Det WD
5.00 kV 3.0 SE 14.4 MIC Cambridge
500 µm

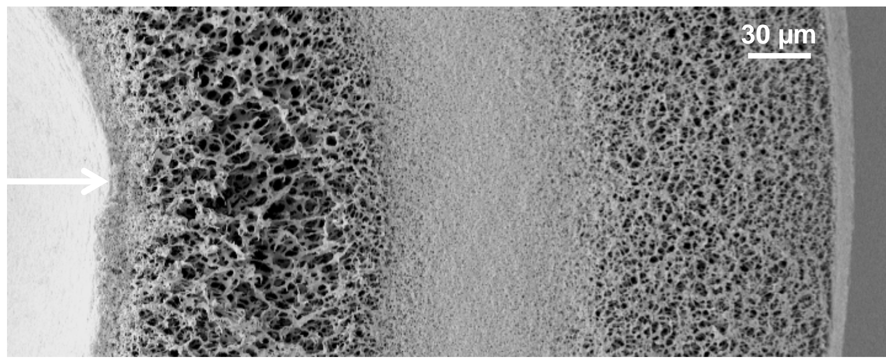
30 µm

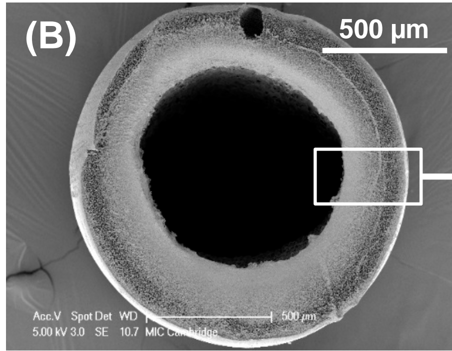
(B)
500 µm
Acc.V Spot Det WD
5.00 kV 3.0 SE 10.7
500 µm

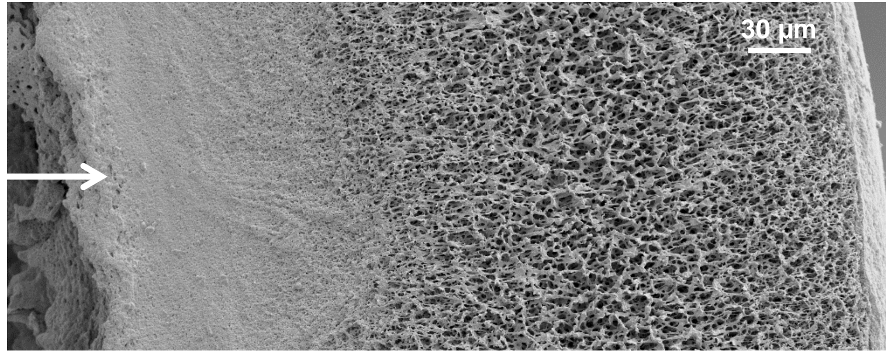
30 µm

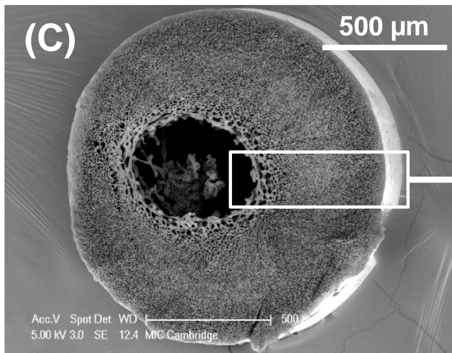
(C)
500 µm
Acc.V Spot Det WD
5.00 kV 3.0 SE 12.4 MIC Cambridge

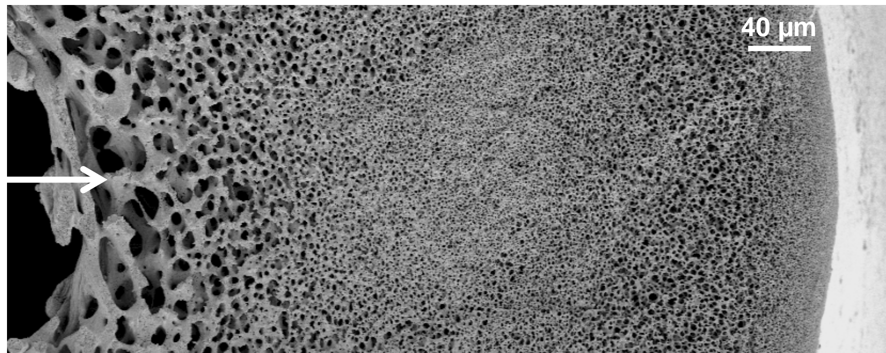
40 µm

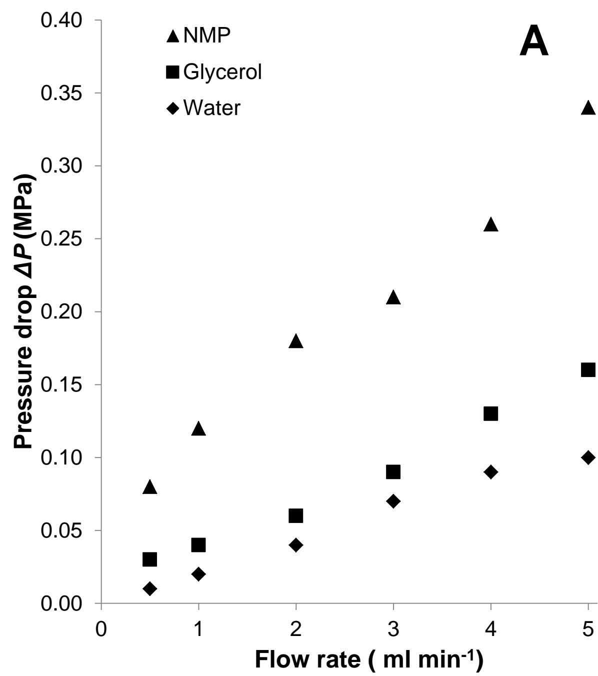
A
NMP
Glycerol
Water
Pressure drop ΔP (MPa)
Flow rate (ml min-1)
0.40
0.35
0.30
0.25
0.20
0.15
0.10
0.05
0.00
0
1
2
3
4
5

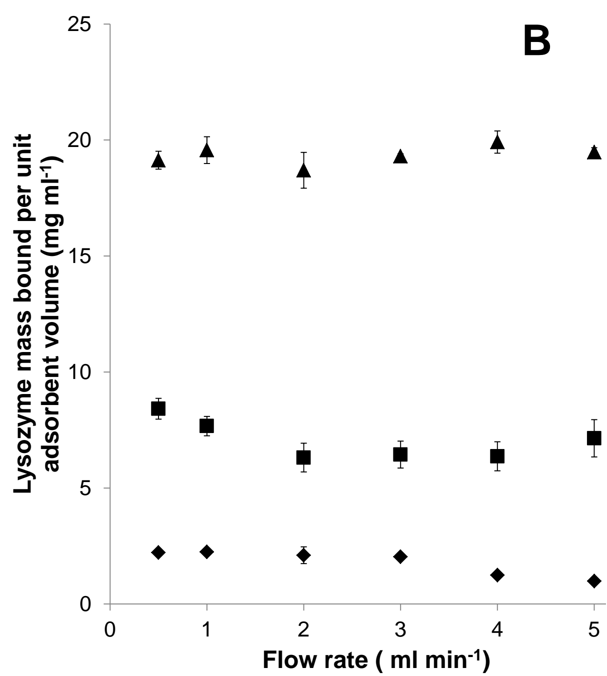
B
Lysozyme mass bound per unit adsorbent volume (mg ml-1)
Flow rate (ml min-1)
25
20
15
10
5
0
0
1
2
3
4
5

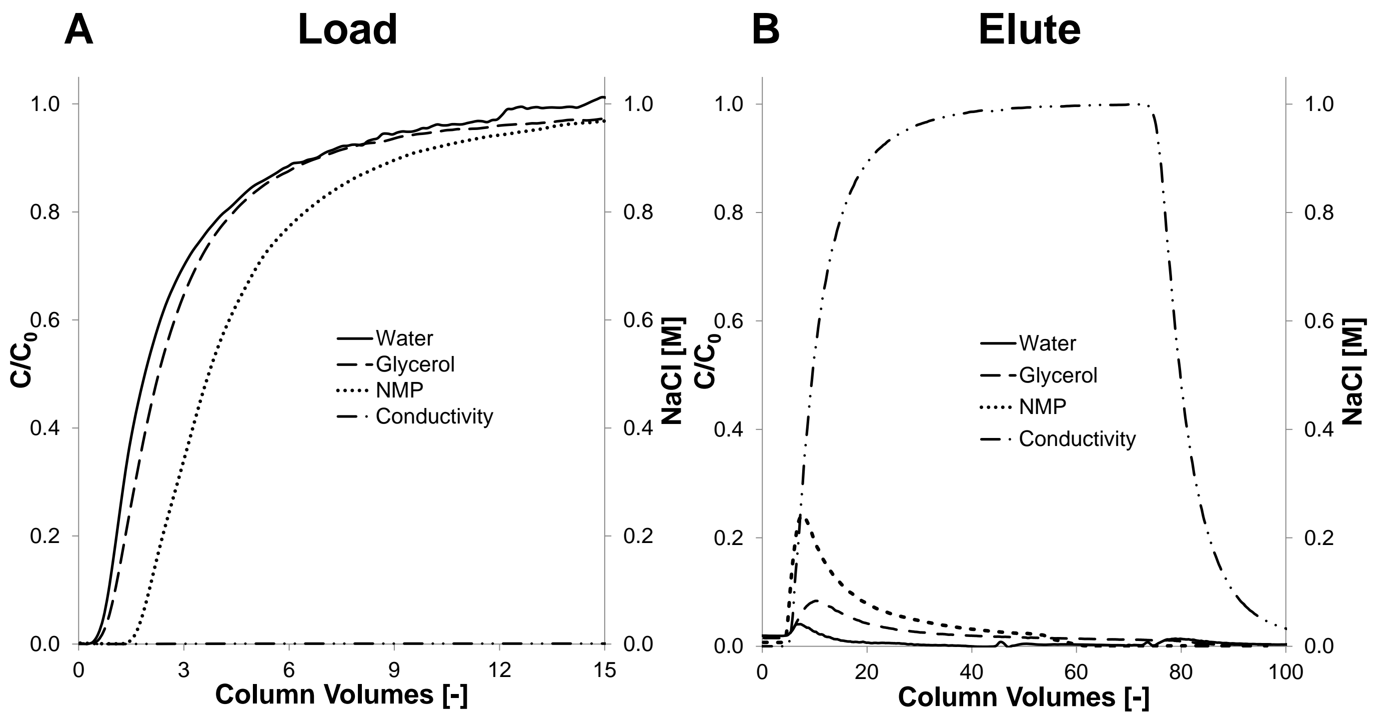
A
Load
C/C$_0$
NaCl [M]
Water
Glycerol
NMP
Conductivity
Column Volumes [-]
B
Elute
C/C$_0$
NaCl [M]
Water
Glycerol
NMP
Conductivity
Column Volumes [-]

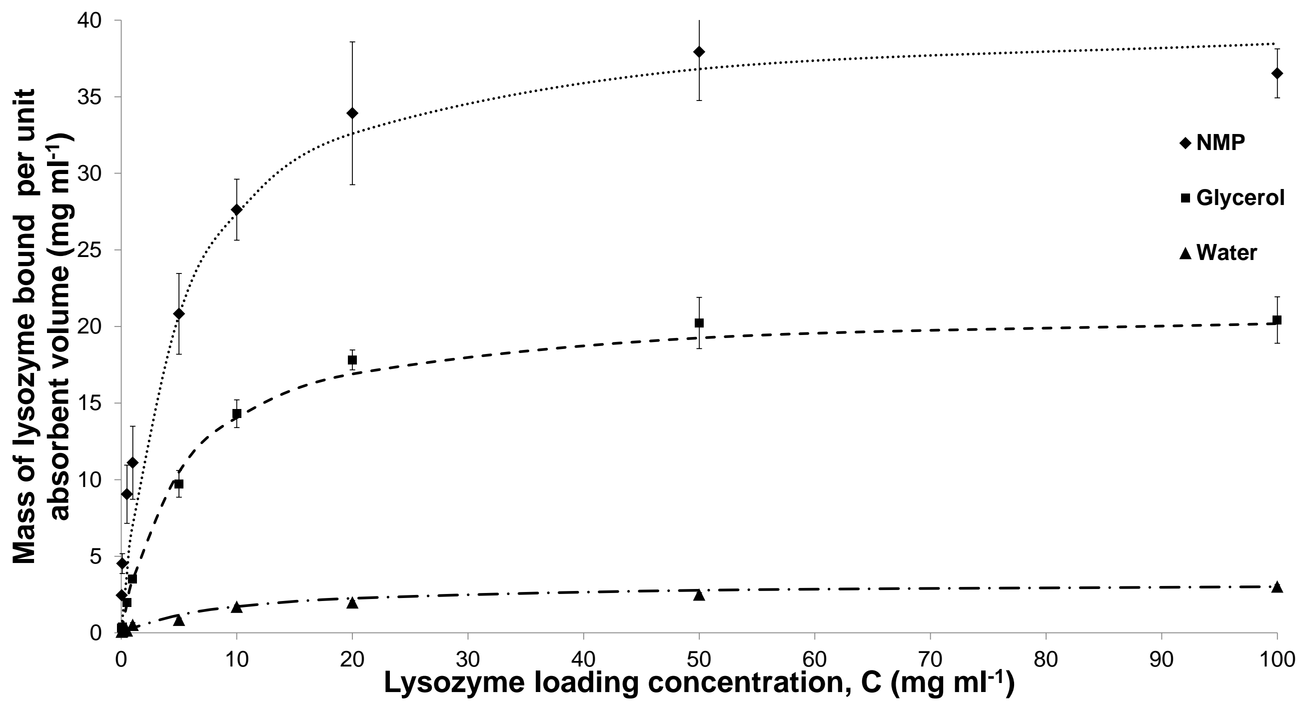
Mass of lysozyme bound per unit absorbent volume (mg ml-1)
Lysozyme loading concentration, C (mg ml-1)
NMP
Glycerol
Water
0
5
10
15
20
25
30
35
40
0
10
20
30
40
50
60
70
80
90
100